Comparative depth-profiling analysis of nanometer-metal multilayers by ion-probing techniques

R. Escobar Galindo, R. Gago, A. Lousa, J.M. Albella

We examine here the depth resolution (interface width) in elemental analysis and depth profiling of complex layer systems of three ion-probing techniques, each of which has pros and cons:

- **Rutherford backscattering spectrometry (RBS);**
- **secondary ion mass spectroscopy (SIMS); and,**
- **glow-discharge optical emission spectroscopy (GDOES).**

RBS is a non-destructive technique that requires no standards for quantification, although access to medium-scale ion-source facilities is needed.

SIMS maintains nanometer (nm) resolution at greater depths but at the expense of longer data-acquisition times.

Finally, GDOES allows depth profiling quickly and accurately, although depth resolution degrades linearly with depth due to sputtering effects (e.g., crater shape and chemical modifications), among other factors.

We discuss these ion-probing techniques in the light of new results obtained with chromium/titanium multilayer structures with individual layer thicknesses between hundreds of nm and a few nm. We resolved ultra-thin chromium layers of 2.5 nm and 5 nm, buried at different depths in titanium matrixes with thicknesses up to 3 μm, and used the results to evaluate the depth resolution of the ion-probing techniques.

Keywords: Depth profiling; Elemental analysis; GDOES; Glow-discharge optical emission spectroscopy; Ion probing; Multilayer; RBS; Rutherford backscattering spectrometry; Secondary ion mass spectroscopy; SIMS

R. Escobar Galindo*, R. Gago, J.M. Albella
Instituto de Ciencia de Materiales de Madrid, Consejo Superior de Investigaciones Científicas, E-28049 Madrid, Spain

R. Escobar Galindo, R.Gago
Centro de Micro-Análisis de Materiales, Universidad Autónoma de Madrid, E-28049 Madrid, Spain

A. Lousa
Departamento Física y Óptica, Universidad de Barcelona, E-08028 Barcelona, Spain

*Corresponding author.
Tel.: +34 914 973 611;
E-mail: ramon.escobar@uam.es

1. Introduction

In recent decades, the use of metal and/or metal-compound multilayer coatings has been extended to an enormous range of applications. By combining synergistically the properties of different materials, it is possible to tune and to optimize desired functional properties. Typical examples involve hard protective coatings for mechanical parts and tools, optical coatings for lenses, filters and architectural glass panels, barrier contacts for microelectronics, quantum superlattices, thermal barriers for gas turbines, thin-film waveguides, and biomedical coatings. In general, for these and other applications, complex coating structures have to be designed in order to accomplish very strict requirements (e.g., thickness homogeneity in the nanometer (nm) range, low surface roughness and abrupt or graded interfaces).

Fig. 1 shows a typical advanced multilayer coating. The first property that any coating should fulfill is good adhesion to the substrate, so it is common in many devices to add adhesive or barrier interlayers (e.g., 50–100 nm of Cr or Ti for metallurgical protective coatings). This buffer layer may also serve as a barrier layer avoiding element inter-diffusion at the film/substrate interface. The structure of the coating itself may comprise a multilayer structure, a graded in-depth composition or even 2D and 3D nanocomposite systems. Of special relevance are multilayer coatings with bilayers of the order of some nm (superlattices), which, among other applications, are designed to reach film hardness in the range of superhard materials (>40 GPa) [1,2], to improve magnetic or transport properties [3,4] or, finally, to tune the optical performance of the films [5,6]. In all these applications, sharp interfaces and a low

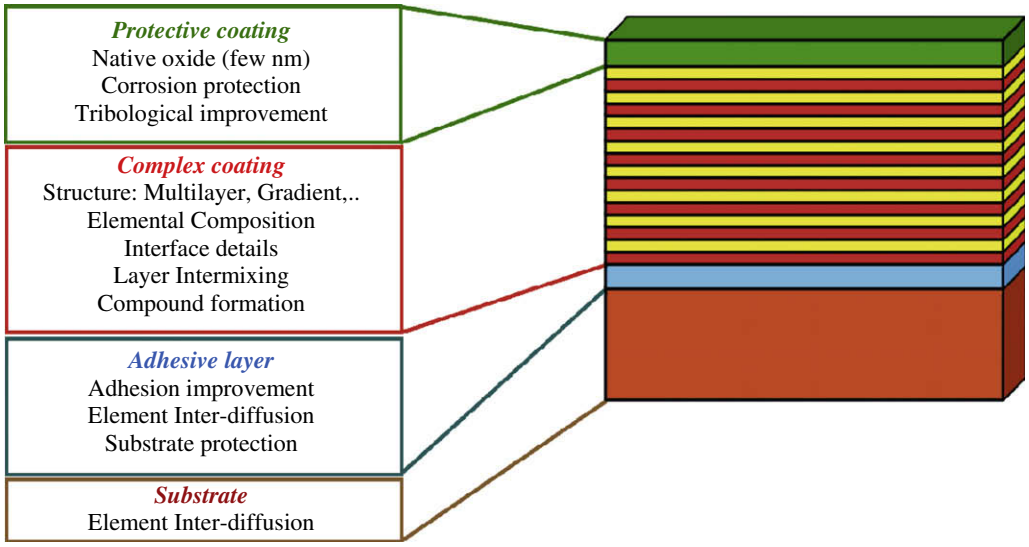

Figure 1. Multilayer coating.

degree of mixing between the component materials are strictly required. Finally, most coatings have a top functional layer to tailor the desired surface properties (e.g., low friction, optical reflectivity, or corrosion resistance).

The analytical characterization of these layered structures requires high-resolution analytical techniques able to provide information about surface and depth composition at the nm level (for references, see the excellent review by Werner and Garten [7]). Well-known techniques [e.g., Auger electron spectroscopy (AES), X-ray photoelectron spectroscopy (XPS), secondary ion mass spectroscopy (SIMS), Rutherford backscattering spectrometry (RBS) and, more recently, glow-discharge optical emission spectroscopy (GDOES)] are generally used for this purpose. In Table 1, the main characteristics of these five techniques are compared. XPS, AES and SIMS suffer from preferential sputtering artifacts. However, in XPS and AES, this effect derives from the analysis of the residual surface composition and, in SIMS, from the flux composition of sputtered ions. Moreover, the maximum depths of analysis of AES and, in particular, XPS are restricted to the sub-μm range, thus limiting the study of thicker coatings. On the other hand, RBS, SIMS and GDOES are all ion-probing techniques capable for analyzing to depths of several μm with nm resolution although without chemical information (as when using XPS and AES). From the above techniques, we have therefore chosen RBS, SIMS and GDOES for the analysis of multilayer systems with individual thickness ranging from a few to some hundreds of nm and a total thickness greater than 1 μm. In the following paragraphs, we briefly describe the principles of the profiling techniques under consideration.

Table 1. Comparative summary of the main characteristics of different surface-analysis techniques

	AES	XPS	RBS	SIMS	GDOES
Excitation probe	Electrons	Photons (XR)	Ions	Ions	Ions
Emission (=detection)	Electrons	Electrons	Electrons	Ions (m/e)	Photons (λ)
Sputtering	Ion beam <10 keV	Ion beam <10 keV	No	Ion beam <10 keV	DC/RF <50 eV
Atom mixing	Yes	Yes	No	Yes	No
Crater effect	No	No	No	Yes (−)	Yes (++)
Max. Depth analysis (μm)	1	0,1	5	5	>100
Depth Resolution (nm)	0.5–2.5	0.5–2.5	5	0.5–2.5	1
Lateral Resolution (nm)	10	10^2	10^5	10	10^6
Chemistry Information	Yes (+)	Yes (++)	No	Yes (+)	No
Detection Limit (ppm)	10^3	10^3	10^3	10^{-1}–10	1
Elemental range	$Z > 2$	$Z > 2$	$Z > 2$	All	All
Calibration Method	Easy	Easy	Standard free	Complex	Complex
Crater diameter (mm)	<1	<1	No crater	<1	4
Vacuum (mbar)	10^{-10}	10^{-10}	10^{-6}	10^{-10}	10^{-2}
Acquisition time	Moderate	Slow	Moderate (minutes)	Slow (hours)	Very fast (seconds)

RBS is a non-destructive technique that is commonly employed for in-depth compositional analysis of metal and metal-nitride layers [8–10]. The technique presents a high elemental sensitivity for heavy elements (<1 at.%) and a depth resolution in the nm range (~5–10 nm), and it does not require standards for quantification. This latter feature makes RBS an excellent candidate to assess the composition of samples to be used later as quantification standards by other techniques (e.g., SIMS or GDOES). Following this idea, Escobar-Galindo et al. [11] have recently implemented a procedure to improve GDOES quantification of nitrogen using home-made nitride coatings as reference materials. The experimental RBS settings (e.g., ion species, and incident energy and angle) are very flexible in order to aim at resolving specific problems. The main drawback of RBS is the requirement for medium-scale instrumentation (e.g., ion implanters or electrostatic accelerators). Other disadvantages include the limitation of the analysis to the very first μm of the sample and the difficulty of detecting light elements on substrates with higher mass number due to a low mass resolution for heavy elements and a low - cross section for low - Z elements. It requires smooth surfaces for analysis and provides no information about the chemical bonding. As we discuss later, there is a decrease of resolution at increasing depths due to energy straggling of the incoming beam.

SIMS equipped with ion-beam depth profiling provides nm resolution at greater depths. This technique is a suitable alternative due to a high level of detection and quantification, lower than 1 ppm, and an excellent depth resolution below 5 nm [12,13]. Nevertheless, such nm depth resolution is only achieved by using primary ion energies in the sub-keV range [14]. However, the advantages of lowering the impact energy are compromised not only by significant surface roughening but also by the decrease in sputtering yield. The small sputtered area allows a lateral resolution of ~5 μm with a dynamic range greater than 10^6 for most elements. Moreover, SIMS is able to discriminate between different isotopes of the same element, although it does not provide information on chemical bonding. It requires ultra-high vacuum (UHV) conditions and the calibration procedure is very complex. The major limitation of the technique is the long experimental time necessary to obtain the spectra since, in routine process development, faster analysis is required to provide feedback information on the effect of the deposition conditions.

GDOES is nowadays a well-established technique capable of overcoming such time-limitation difficulties [15,16]. The method is based on detection of the light emitted from the excited atoms sputtered from the sample surface by a glow discharge. Only moderate vacuum is required, and erosion and sampling rates are high enough (typically >1 μm/min) to obtain a compositional profile of some μm in depth in a few minutes, with a depth resolution in the nm range [17–20] and a high level of detection (1 ppm) and quantification (10 ppm). Besides, the use of a radiofrequency (rf) source for sputtering extends the application of GDOES to the study of insulators as both coatings and substrates [21,22]. Hydrogen can be detected by GDOES, although it requires corrections to be applied due to changes in the emission lines [23,24]. However, GDOES is a destructive technique that does not provide any chemical information and, due to the large crater area (4 mm), has no lateral resolution. There are serious problems associated with crater geometry, which, in certain applications, has to be optimized to reduce the loss of resolution with depth, (as discussed in [25–29]) Finally, the calibration procedure for GDOES is complex and the lack of reference materials limits the quantitative analysis of important elements (e.g., oxygen, nitrogen or hydrogen), typically found in many coating structures. This specific issue has been discussed in detail elsewhere [11,30,31].

Although there has been extensive work on depth resolution in multilayers (mostly in metal systems) [32–44], there has been no systematic work comparing the depth-profiling performance and the accompanying effects on the widening interface of RBS, SIMS and GDOES techniques. We focus the discussion on periodic metal layers as ideal cases of more complex structures generally used in mechanical, optical, electrical and magnetic applications, where binary or ternary metal compounds are generally employed (oxides, nitrides and carbides of transition metals).

2. Experimental

2.1. Metal-multilayer-coating deposition

Cr, Ti and Al multilayer coatings with individual thickness in the range 2.5–700 nm and different material sequences were deposited to compare the composition depth profiles, as obtained from GDOES, RBS and SIMS, and to explore the resolution limits of the techniques. The deposition of the multilayers was performed in a conventional planar DC magnetron sputtering system using two sputtering sources, placed 6.5 cm from the substrate holder. The holder can be rotated to face the sample to each sputtering source in turn and is provided with automatic position controller in order to control the deposition time for each layer. The deposition rates of the specimens were 12.5 nm/min for titanium, and 25.0 nm/min for chromium and aluminum. Details of the sputtering system have been described elsewhere [45]. The base pressure was approximately 2×10^{-4} Pa and the working pressure was in the range 0.16–0.23 Pa. The cathode power was held constant at 100 W. No bias voltage was applied to the substrate holder. Prior to deposition, 20 min of pre-sputtering was performed in order to clean the cathodes of previously

Table 2. Description of coating systems studied. All coatings were deposited onto (100) silicon

Sample	Thickness (μm)	Coating structure
Thick trilayer	1.5	700 nm Ti/700 nm Cr/700 nm Ti
	1.3	450 nm Cr/400 nm Al/450 nm Cr
Thin multilayer	2.2	10× (65 nm Ti/140 nm Cr)
	2.2	10× (80 nm Cr/140 nm Ti)
Ultra-thin multilayer	3	6× (5 nm Cr) @ Ti matrix
	3	7× (2.5 nm Cr) @ Ti matrix

deposited materials. The metal targets used were commercial plates of very high purity. Very pure Ar (99.999%) was introduced into the vacuum chamber as reactive gas. The coatings were all deposited onto Si (100) substrates. Table 2 gives a summary of the coatings studied in this work.

2.2. Multilayer characterization

The shape and depth of the sputtering crater and the coating thickness were measured by profilometry utilizing a Dektak 3030 surface profilometer. Scanning electron microscopy (SEM) micrographs of the multilayer structure were obtained by a Hitachi S-2700 model using an accelerating potential of 15 kV. Cross-sectional transmission electron microscopy (TEM) micrographs were obtained using a Jeol 4000 EX/II model with an accelerating potential of 400 kV.

RBS experiments were performed with the 5 MV HVEE Tandetron at the Centro de Micro-Análisis de Materiales [46] of Universidad Autónoma de Madrid, Spain. The RBS spectra were collected with He ions at an ion dose of 10 μC and ion energies of 1.5, 2 and 3.5 MeV. The analysis at different ion energies provided complementary information about the coating structure (i.e. higher surface sensitivity at 1.5 MeV whereas higher penetration depth together with non-Rutherford cross-section ($\sigma \sim 2\sigma_R$) [47] for the $^{14}N(\alpha, \alpha)^{14}N$ process was achieved at 3.5 MeV). The data were acquired simultaneously with two silicon surface-barrier detectors located at scattering angles of 170° and 165°, respectively, and with an energy resolution of 15 keV. The experimental spectra were fitted with the SIMNRA program [48].

GDOES depth-profile analysis of the coatings was completed using a Jobin Yvon RF GD Profiler [49] equipped with a 4-mm diameter anode and operating at a typical rf discharge pressure of 650 Pa and power of 40 W. The samples were cooled using a re-circulating water system to avoid heating effects during the GDOES experiments. The chamber was cleaned by sputtering a silicon (100) sample for 20 min. Before every experiment, the samples were flushed with argon for 60 s. The sputtering rates of the studied elements were measured to be of 5.3, 5.4, 3.5 and 3.4 μm/min for chromium, aluminum, titanium and silicon, respectively. The high etching rates obtained during GDOES analysis resulted in very short experimental times (below 1 min of operation). A collection rate of 200 points/s was used to measure all the samples. Quantified profiles were obtained automatically using the standard Jobin Yvon Quantum Intelligent Quantification (IQ) software, and the set-up was calibrated using standard materials of known composition.

SIMS analyses were performed using an Atomika 488 system. Analyses were carried out at a vacuum of under 10^{-8} Torr. O_2^+ molecular ions at 12 keV were used to sputter an area of 350 μm × 350 μm and positive secondary ions were collected from the central region using 20% of electronic gate to avoid the crater edge effects. All the measured species were detected as elemental ions. Certainly, 12 keV was too high to expect excellent depth resolution, especially when detecting very thin layers, but 12 keV was chosen as a reasonable compromise in order to keep the SIMS analysis time of our samples (several μm thick) within a reasonable time of a few hours. The X-axis co-ordinate of SIMS profiles was converted from sputtering-time data to depth-from-the-surface data by measuring the depth of sputtered craters using a DEKTAK-3 surface profilometer.

3. Results and discussion

3.1. Thick metal multilayers (thickness ~500 nm)

Fig. 2 shows the depth profiles of a Ti/Cr/Ti trilayer deposited on Si(100), as measured by a) RBS, b) GDOES and c) SIMS. The total thickness of the coating was 2.1 μm with each individual layer 700 nm thick, as measured by SEM and profilometry. We describe these spectra in the following paragraphs.

For clarity, the RBS experimental data and the global fitting of results were shifted vertically from the contributions of the elemental spectra (lower part of the graphs) in Fig. 2(a). RBS fitting of the experimental results gave very good agreement with the nominal layer thickness (~600 nm for each individual layer) and showed a very well-defined coating structure with sharp interfaces down to the limit of the technique (i.e. $\pm 50 \times 10^{15}$ at/cm^2 or ~5 nm). A small amount of oxygen contamination (<10%) was detected in the Ti layers only, being higher for the layer at greater depth (closer to the substrate). This suggests that oxygen was incorporated from the residual gas and was consumed progressively.

The GDOES spectrum of the Ti/Cr/Ti stacking (Fig. 2(b)), although showing very square profiles and excellent agreement with the individual layer thicknesses (650/600/650 nm), displayed typical GDOES features affecting the depth resolution of the technique.

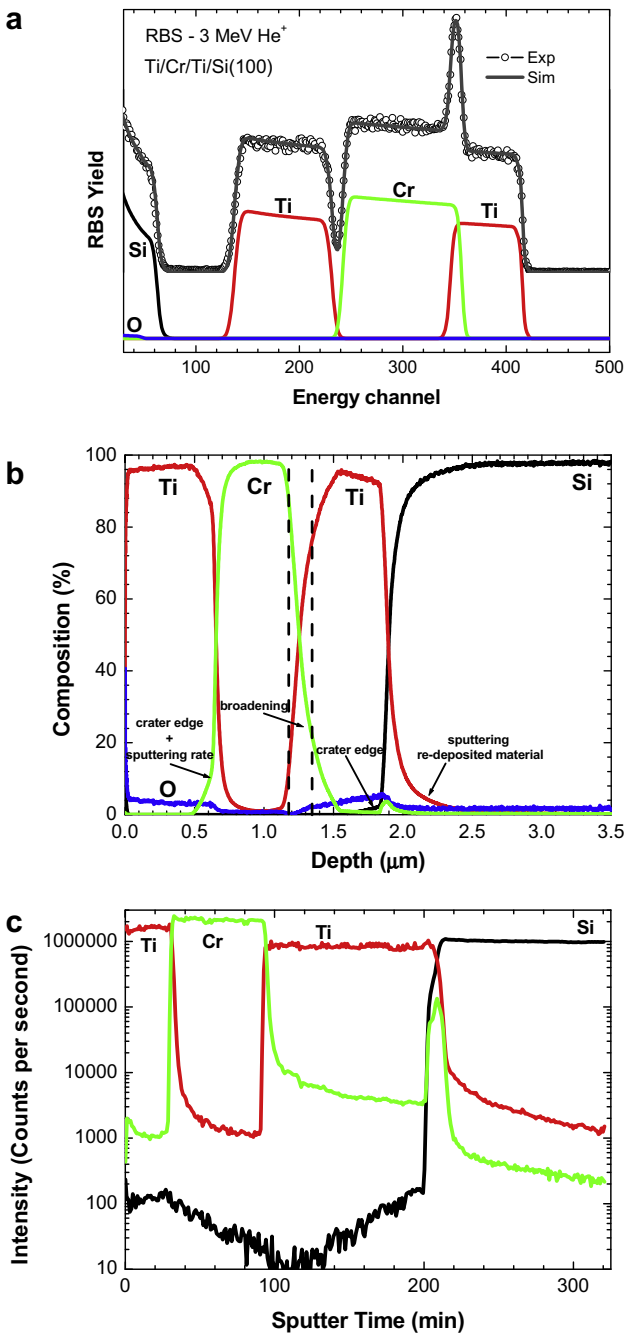

Figure 2. Depth profile of a trilayer 700 nm Cr/700 nm Ti/700 nm Cr by a) RBS, b) GDOES and c) SIMS. In a), the experimental data and the global fit results have been shifted vertically from the contributions of the elemental spectra (lower part of the graphs). The dashed vertical lines in b) indicate the broadening of the Cr/Ti interface. Note that, in c), the vertical axis (intensity) is in logarithmic scale.

These artifacts were mainly due to the non-flat geometry of the sputtering crater (i.e. the presence of a well at the edge of the crater, which was extensively studied in previous works [25,26]). Due to these artifacts, the interfaces between the metal layers linearly broaden with depth. Applying ''the inverse slope'' method to the Ti/Cr/Ti system to determine the depth resolution of the GDOES profiles [50], the first Ti/Cr interface (at 650 nm) was measured to be of 57 ± 4 nm, the subsequent Cr/Ti interface (at 1.25 μm) broadened to 193 ± 14 nm and finally the Ti/Si interface was found to be of 101 nm ± 7 nm. Despite the lack of oxygen-containing standards for GDOES calibration, it was remarkable how the titanium getter effect was clearly observed in the GDOES profile with a small concentration of 3–5 at.%. The oxygen contamination increased for inner layers, as assessed by RBS.

In the SIMS profile of Fig. 2(c), it can be appreciated that the times required to sputter each titanium layer were not equal. This meant that, during the experiment, the titanium sputtering rate changed from 22 nm/min for the first layer to 6 nm/min for the second one. The measurement was repeated and the same result was obtained. This strong reduction of the sputtering rate was accompanied by a reduction of almost half of the Ti^+ signal from the most superficial layer (1.6×10^6 counts) to the buried one (8.4×10^5 counts), suggesting a progressive decrease of the effective oxygen ion-beam intensity during the long experimental time (more than 3 h) required for the analysis. Nevertheless, this effect seems to be specific to Ti, as it was not observed in other materials, and was probably associated with the high solubility of oxygen in titanium and the complex matrix effects that may occur in this material at even moderate oxygen concentrations. Despite the changes in the sputtering rate, the interfaces measured by SIMS were constant with depth and sharper than in GDOES (Ti/Cr: 40 ± 22 nm, Cr/Ti: 30 ± 11 nm and Ti/Si: 28 ± 6 nm, as derived from the 84–16% rule [42]). The interfaces Ti/Cr and Cr/Ti are very asymmetric: tails of composition appear only in the direction of progress of the analysis, and can be attributed to a mixing effect caused by the bombarding oxygen ions. The absence of appreciable tails of composition in the opposite direction is a clear indication that the interfaces are very steep, with very low values of interdiffusion and/or roughness. Finally, it is remarkable that, at the Ti/Si interface, the chromium signal increased. The use of logarithm scale in Fig. 2(c) may, at first sight, cause the relevance of the observation to be overestimated. The chromium intensity at the interface with silicon, although not negligible, represented only 5% of the intensity of the Cr intermediate layer. The drift of Cr material to the interface was due to ion sputtering and this effect was enhanced by the change of matrix at the Ti/Si interface. A similar behavior has been observed systematically in other multilayer systems (e.g., CrN/CrC or Cr/CrC) [51].

The Ti/Cr/Ti trilayer described above represents a near-ideal system with very sharp interfaces and constant thickness and composition, so any discrepancy between this structure and the experimental depth pro-

file obtained must be attributed to degradation in the depth resolution determining the performance of the technique used in the analysis.

However, as in practice most systems show rough interfaces and element inter-diffusion, a comparison of the techniques in non-ideal systems is highly recommended. This is the case for aluminum films. In previous unpublished work, a 1-μm aluminum layer was deposited on silicon showing a very high roughness of ~200 nm, so it was expected that, in a multilayer system containing Al stacks, the interfaces would be much broader than in the previous Ti/Cr/Ti system.

Fig. 3 shows the depth profiles of a Cr/Al/Cr trilayer. The total thickness of the coating was 1.3 μm with each Cr layer 450 nm thick and the intermediate Al 400 nm thick, as measured by SEM and profilometry. Fig. 3(a) shows the RBS experimental and fitting spectra. The layer thicknesses obtained from the simulation was 550 nm for the Cr layers and 600 nm for the intermediate Al layer, slightly shifted from the nominal values, since we assumed the density of bulk materials. A small amount of oxygen contamination (<10%) was found in the Al layer. The simulation results for the Cr/Al/Cr systems showed that the interface widths were slightly broader (a few nm) than in the case of Ti/Cr/Ti. This may be related to the Al layer being very rough.

The influence of the roughness of the Al layer was unambiguously observed in the GDOES and SIMS spectra of Fig. 3(b) and (c). The GDOES signal of the aluminum layer shows a non-square profile with very different Cr/Al and Al/Cr interfaces of 125 ± 9 nm and 84 ± 6 nm, measured at 490 nm and 1 μm, respectively. It is important to note that, as both Al and Cr have very close sputtering rates and develop a similar crater shape, the Cr/Al and Al/Cr interfaces should have shown an analogous linear broadening with depth [25]. The fact that the first Cr/Al interface is much broader than the buried Al/Cr is a clear indication that the aluminum layer was very rough (>90 nm). However, the chromium profiles were very square with excellent agreement with the layer thickness (490/510/600 nm). A very small amount of oxygen (<1 at.%) was measured in the Cr/Al/Cr trilayer in contrast with the Ti/Cr/Ti system.

The SIMS profile of Fig. 3(c) shows that the sputtering rates were constant for both Cr layers (10 nm/min) and very similar to the aluminum sputtering rate (8 nm/min). Inside each layer, the signal from the materials layer was up to 1000 times higher than the signal corresponding to the adjacent layers. This factor of 1000 was similar to that observed in the previously studied Ti/Cr/Ti trilayer, and was much higher than that observed in the GDOES analysis. However, the apparent thicknesses of the interfaces were: 47 ± 8 nm for Cr/Al, 12 ± 7 nm for Al/Cr and 24 ± 8 nm for Cr/Si. The main difference with the case of the Ti/Cr/Ti trilayer lies in the behavior of the tails of intermediate material at the two

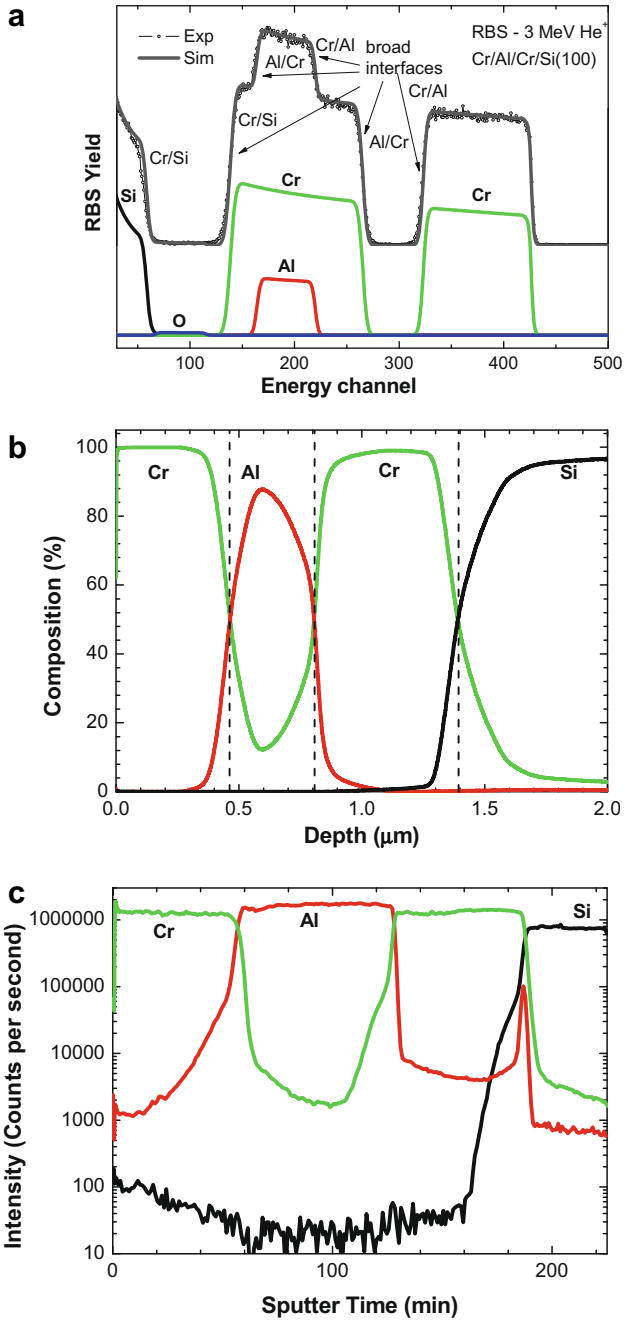

Figure 3. Depth profile of a trilayer 450 nm Cr/400 nm Al/450 nm Cr by a) RBS, b) GDOES and c) SIMS. In a), the experimental data and the global fit results have been shifted vertically from the contributions of the elemental spectra (lower part of the graphs). The dashed vertical lines in b) indicate the location of the different interfaces. Note that, in c), the vertical axis (intensity) is in logarithmic scale.

interfaces. The Al tail in inner Al/Cr interface was very short while the Al tail in the outer Cr/Al interface was long towards the external surface. This behavior was just the opposite of that we might expect from the effect of mixing the bombarding ions of the SIMS analysis, and

can be attributed to the Cr/Al interface being very rough through the growth of the 600-nm Al layer on a relatively flat 580 nm Cr layer on silicon. Finally, and similarly to the above observation, there was a drift of Al material (∼5%) to the Cr/Si interface due to the ion sputtering.

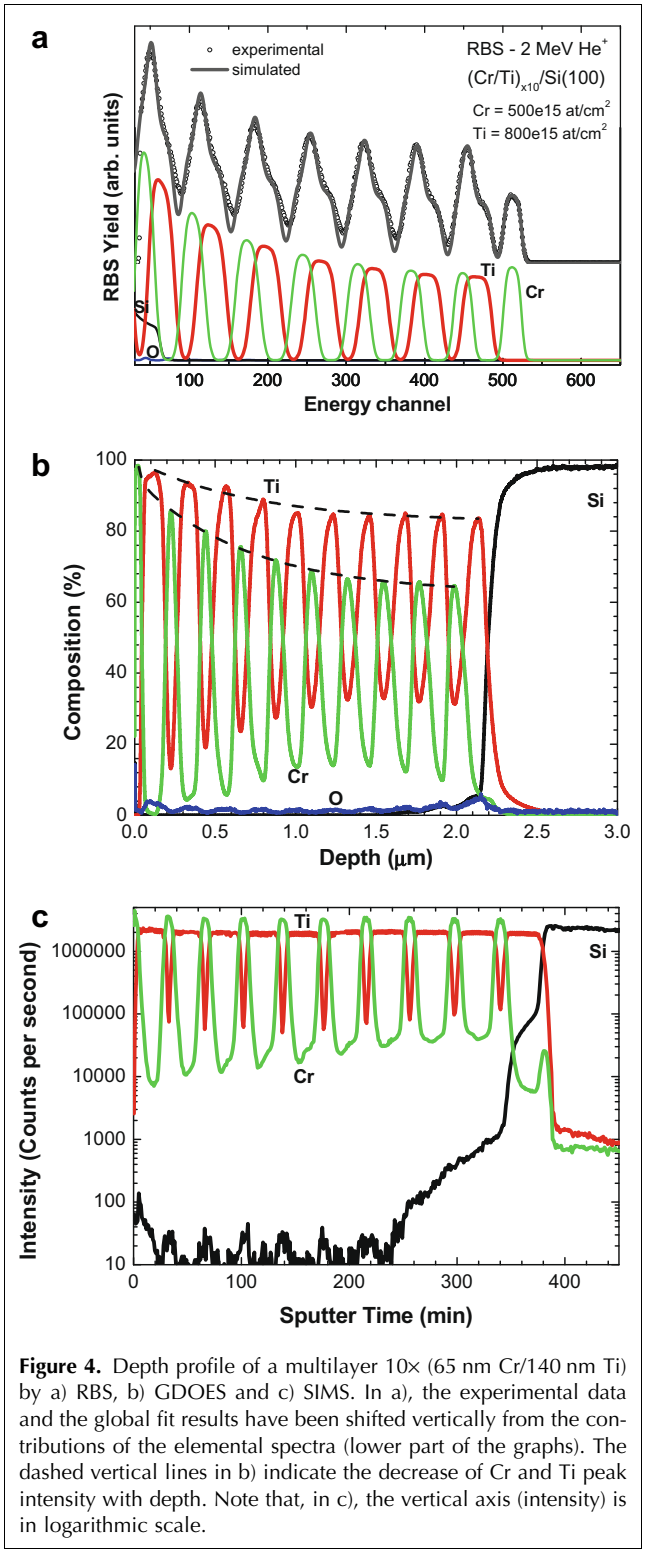

Figure 4. Depth profile of a multilayer 10× (65 nm Cr/140 nm Ti) by a) RBS, b) GDOES and c) SIMS. In a), the experimental data and the global fit results have been shifted vertically from the contributions of the elemental spectra (lower part of the graphs). The dashed vertical lines in b) indicate the decrease of Cr and Ti peak intensity with depth. Note that, in c), the vertical axis (intensity) is in logarithmic scale.

3.2. Thin metal multilayers (thickness ∼100 nm)

The depth profiles of multilayer systems comprising 10 alternate Cr and Ti layers of nominal thickness of 65 nm and 140 nm, respectively (Fig. 4) and the reverse system

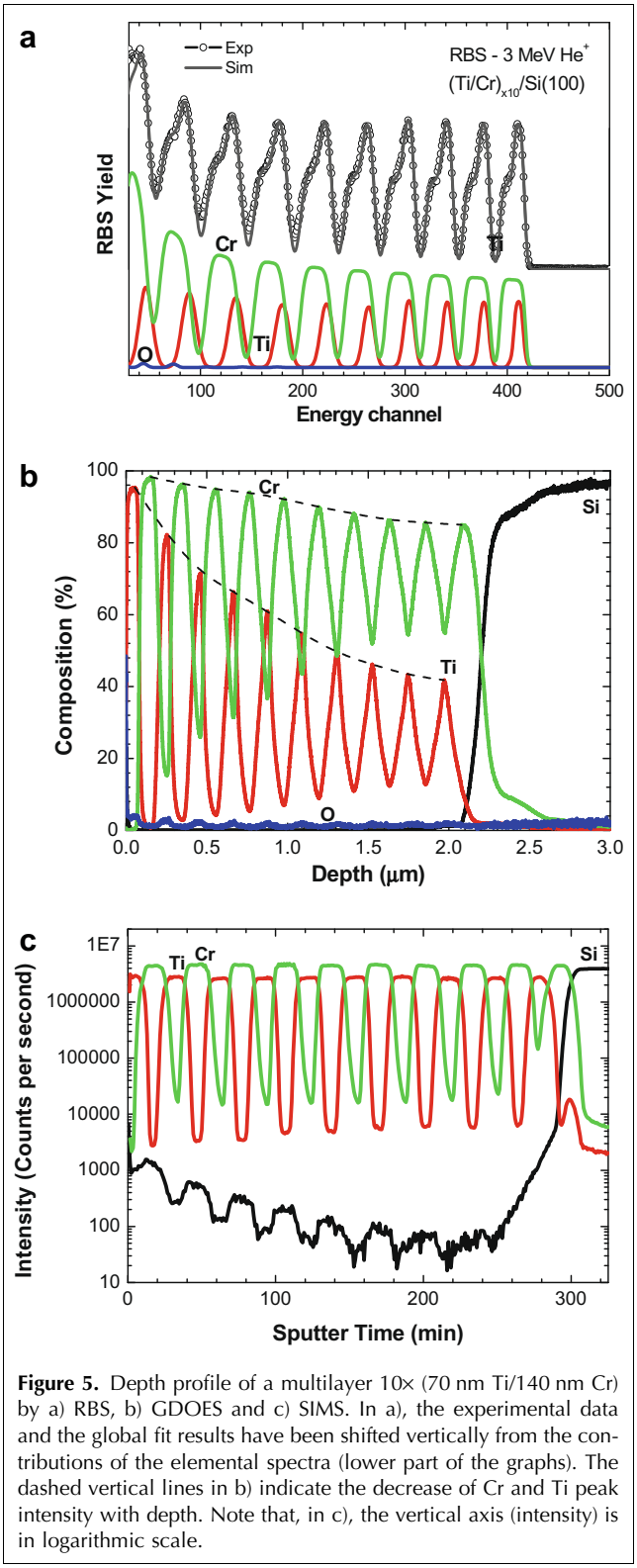

Figure 5. Depth profile of a multilayer 10× (70 nm Ti/140 nm Cr) by a) RBS, b) GDOES and c) SIMS. In a), the experimental data and the global fit results have been shifted vertically from the contributions of the elemental spectra (lower part of the graphs). The dashed vertical lines in b) indicate the decrease of Cr and Ti peak intensity with depth. Note that, in c), the vertical axis (intensity) is in logarithmic scale.

of 10 alternate Ti and Cr layers of nominal thickness of 80 nm and 140 nm, respectively (Fig. 5) are shown as measured by a) RBS, b) GDOES and c) SIMS. The individual layer thicknesses were measured by cross-sectional TEM.

The oscillations in the RBS spectra (Figs. 4(a) and 5(a)) reflect the layered structure of the coating, the signals from each individual layer being clearly resolved in the elemental spectral contribution (bottom parts of the figures). The simulation of the RBS spectra given by a sequential bilayer system perfectly reproduced the experimental data in Figs. 4(a) and 5(a). In addition, the thickness values extracted from the simulation were in excellent agreement with the nominal thicknesses of the layers (see Fig. 6). Mean thickness values of 58 ± 5 nm and 130 ± 6 nm for Cr and Ti layers, respectively, were found for the 10× Cr/Ti system. In the 10× Ti/Cr coating, the RBS analysis gave mean values of 75 ± 3 nm and 136 ± 4 nm for Ti and Cr, respectively. The simulated spectra, assuming pure layers, accurately fitted the data, indicating very sharp interfaces in both cases. Furthermore, experiments at an incident angle of 45° were carried out to estimate the interface thickness by comparing the thicknesses of the first five layers at 0° and 45°. Similar Cr/Ti and Ti/Cr interfaces of 6–8 nm were found, remaining practically constant with depth. Around a depth of 1 μm, there was a slight increase in the interface but was considered to be due to the contribution of energy straggling and multiple scattering at greater depths. This increase could be related to the oxygen content detected in the inner Ti layers.

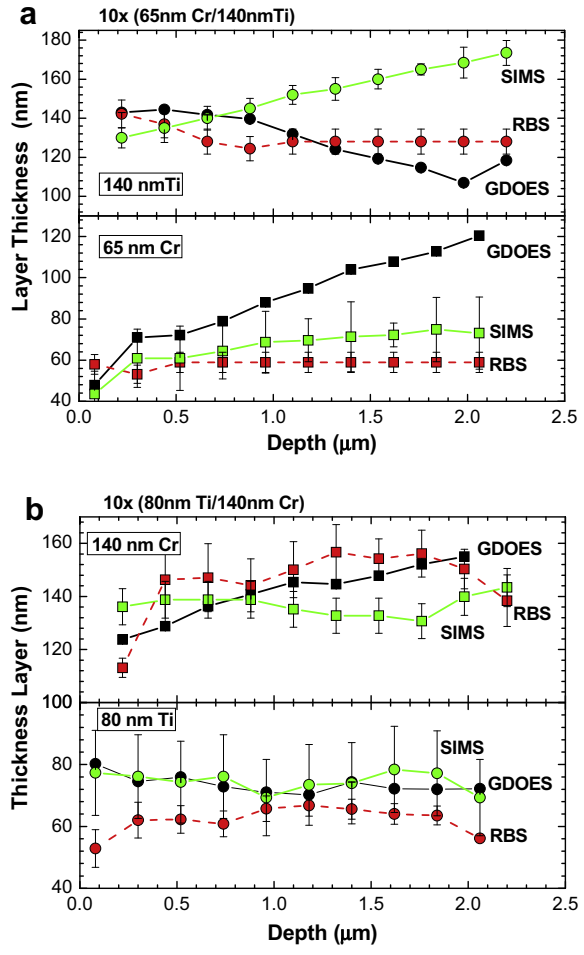

Figure 6. Variation of the individual metal-layer thickness with sputtering depth for multilayers a) 10× (65 nm Cr/140 nm Ti) and b) 10× (70 nm Ti/140 nm Cr), as measured by RBS (open symbols), SIMS (gray symbols) and GDOES (black symbols).

Although the GDOES profiles perfectly reproduced the bilayer composition of both thin metal multilayer systems, as discussed in [26], the results were very dependent on the order on the layers XY (i.e. X/Y ≠ Y/X). In the profile of the 10× Cr/Ti system (Fig. 4(b)), there was a decrease in the intensities of both 65-nm Cr (down to 65%) and the 140-nm Ti layers (down to 84%). There was clearly layer intermixing as the thickness of the thin Cr layer, as measured by GDOES, increased monotonously up to 120 nm, while the thickness of the thick Ti layer decreased to 105 nm (see Fig. 6(a)). The bilayer period was kept constant within the overall coating. However, in the 10× Ti/Cr profile (Fig. 5b), there was severe degradation of the Ti signal down to 40% while the Cr signal slightly decreased to 90% for the last layer. Regarding the individual layer thickness, it can be observed in Fig. 6(b) that there was good correlation with the nominal thickness for both Ti (74 ± 3 nm) and Cr (142 ± 10 nm) layers. The way that the differences observed in the profiles depended on the order of the layers was discussed in [26], in terms of the different erosion rates and thicknesses of the Cr and Ti layers. Recently, we have properly simulated this phenomenon using a simple model of degradation of the layer interfaces induced during analysis by the ion bombardment and subsequent erosion of the surface atoms [52].

The SIMS profiles of Figs. 4(c) and 5(c) reveal a constant composition (changes are below 5 at.%) of the layers regardless of the order of the materials. In the profile of the 10× Cr/Ti system, there was an increase in layer thickness measured for both elements (Fig. 6(a)). This might be related to changes of the sputtering rate during SIMS analysis, as explained above. However, the 10× Ti/Cr system showed a constant layer thickness for both Ti (62 ± 4 nm) and Cr (145 ± 12 nm) layers, as observed in Fig. 6(b). Cr/Ti and Ti/Cr interface widths were measured as being similar (32 ± 7 nm).

3.3. Ultra-thin metal multilayers (thickness <5 nm)

In order to compare the performance of RBS, GDOES and SIMS during the analysis of multilayers in the nm range, two different systems were studied. First, a multilayer system comprised six 5-nm thick layers of Cr deposited at

depths of 0.05, 0.1, 0.25, 0.5, 1 and 2 μm from the coating surface. Second, we deposited a similar multilayer of six 2.5-nm thick Cr layers at the same depths as above, plus an extra marker at the outermost surface. In both cases, the Cr markers were buried between Ti layers of variable thickness with a total coating thickness of 3 μm (see Table 2).

The six 5-nm Cr markers were perfectly identified in the depth profiles by the three techniques, even when embedded a few μm deeper into the Ti matrix, with excellent correlation between the estimated depth of the markers and those measured. Near the outermost surface (see Fig. 7), the first two markers, although detected, were not well resolved because of their proximity (50 nm). Nevertheless, the SIMNRA software allowed the RBS profile to be simulated and perfectly resolved all the markers. No degradation in either intensity or layer thickness was found in the RBS analysis. In particular, it is interesting to note the excellent agreement with the marker thickness of 4.8 ± 1.2 nm (see Fig. 8).

During the GDOES analysis, the six Cr markers were unambiguously observed [26], but there was a clear degradation in both intensity and thickness of the layers. The heights of the Cr peaks decreased with depth (see dashed line in Fig. 7(b)) from 35 at.% at 50 nm to less than 10 at.% at 2 μm, while the measured layer thickness increased from 30 nm up to 130 nm (Fig. 8). The analysis of the GDOES depth profiles could be enormously improved by applying deconvolution algorithms (i.e. Van Citter or Gold [53–55]). Currently, this is a very active topic within the GDOES community, and there have been some attempts to apply such algorithms to GDOES analysis [26,44].

In the SIMS depth profile, the thin Cr markers were observed as Gaussian-like peaks because their thickness (5 nm) was much less than the depth resolution corresponding to parameter analysis. There is practically no degradation of the Cr peaks, except for the first marker. This marker, located at 50 nm from the surface, had almost double the intensity and a lower width (12 nm) than the rest (36 nm), and it was found at a sputtering time shorter than that corresponding to the average sputtering rate of 6.1 nm/min (Fig. 7c). The behavior of this first marker can be explained by the so-called ''transient effect'' due to non-stabilized oxidation during the first stages of the SIMS erosion process, which led to higher sputtering and ionization yields [56]. For the rest of the markers, the intensity remained constant within an error of 10%, and the peak thickness was stable around a value of 36 ± 2 nm (see Fig. 8). The width of the surface region affected by the transient effect could be thus estimated to be around 70 nm for our experi-mental conditions.

Finally, we compared the depth-profile results on the second 2.5-nm Cr marker system in order to evaluate the ultimate depth resolution of the techniques.

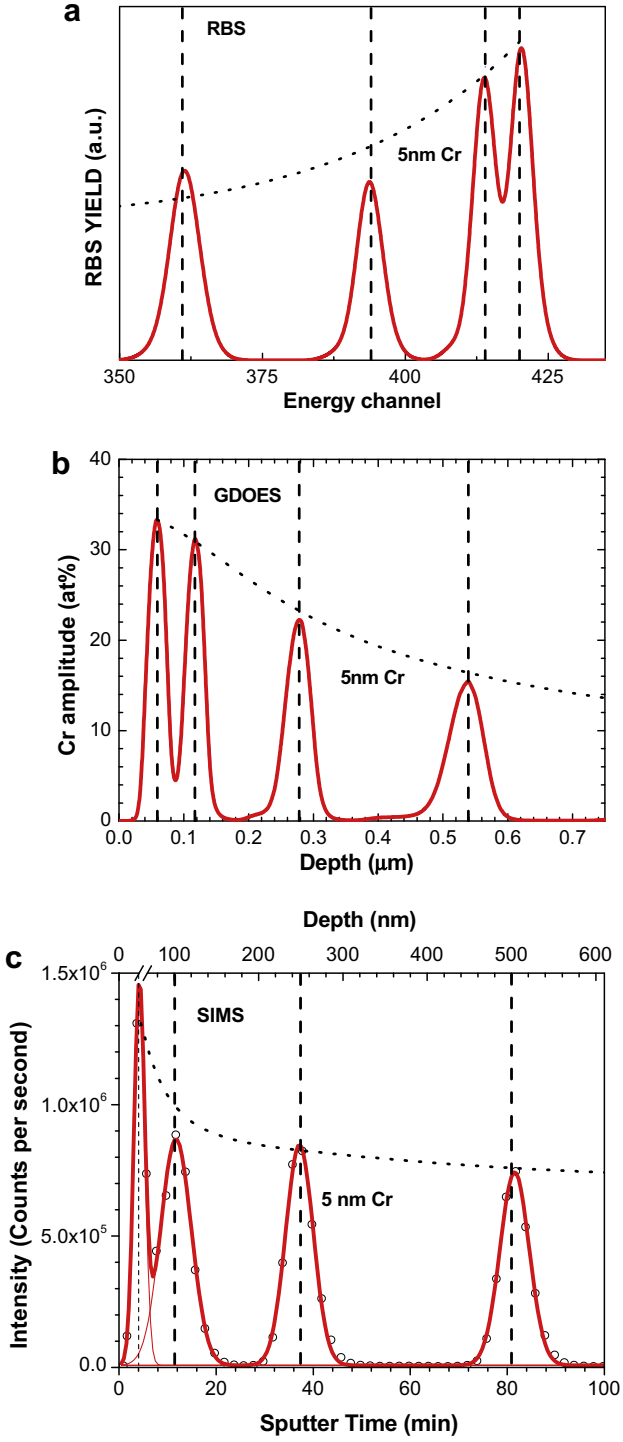

Figure 7. Depth profile of a multilayer coating consisting of 10× 5 nm Cr layers (markers) embedded in a Ti matrix by a) RBS, b) GDOES and c) SIMS. Only the first four Cr layers are shown. The dotted lines follow the variation of the chromium peak intensities with depth and the dashed vertical lines indicate the position of the markers.

RBS experiments did not resolve any of the 2.5-nm layers, confirming that the depth resolution of this

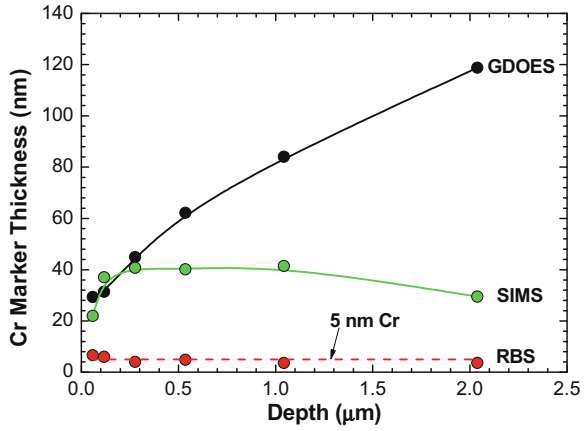

Figure 8. Variation of the thickness of the Cr marker embedded in a Ti matrix with sputtering depth, as measured by RBS (open symbols), SIMS (gray symbols) and GDOES (black symbols).

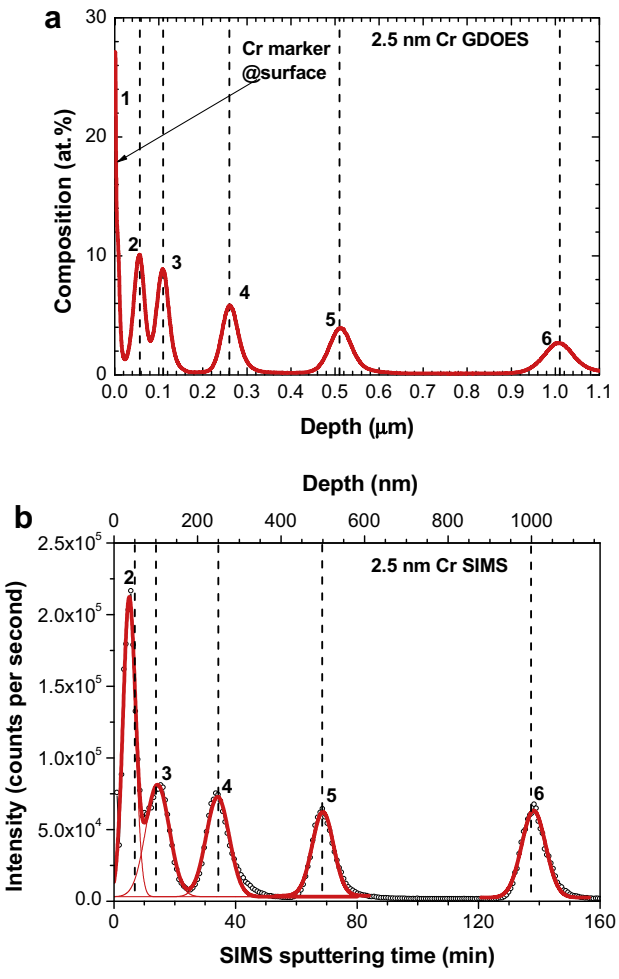

Figure 9. Depth profile of a multilayer coating consisting of 10× 2.5 nm Cr layers (markers) embedded in a Ti matrix by a) GDOES and b) SIMS. Only the first six Cr layers are shown. The dashed vertical lines indicate the position of the markers.

method in this system is no better than 5 nm. In recent years, a great effort has been made to develop high-resolution RBS systems (HR-RBS) by using magnetic spectrometers [57–59]. HR-RBS measurements of ultra-thin layers at nm or even sub-nm scale have been reported recently [60,61].

However, both GDOES and SIMS were able to detect the ultra-thin Cr layers but with different sensitivities. GDOES resolved the seven 2.5-nm markers, including the one deposited on the outermost surface, but showed pronounced degradation of the profiles, as observed in Fig. 9(a). The peak intensities decrease from 30 at.% at the surface down to 2 at.% at a depth of 2 μm with layer thickness increasing from 14 nm to 80 nm. By contrast, the SIMS depth profile showed a similar behavior to that observed for 5-nm Cr markers. No degradation was observed in the Cr peaks located at depths below 50 nm from the surface (Fig. 9(b)), as both the intensities and the peak width (54 ± 3 nm) remained constant for the rest of the peaks. The two markers located near the surface (at 0 and 50 nm) were modified by the transient effect. The first marker was practically lost, while the second was found at a sputtering time shorter than that corresponding to the average sputtering rate of 7.3 nm/min. As in the case of the 5-nm layers, there was excellent correlation between the nominal depth of the 2.5-nm markers and those measured by GDOES and SIMS.

4. Conclusions

From the above results, we can conclude that RBS, GDOES and SIMS are suitable and complementary techniques for in-depth elemental analysis of metal-multilayer stacks of nm individual thickness. Very good correlation between nominal thickness and calculated values were found by the depth profiles obtained using the three techniques, though the analytical method was very different in each case.

RBS, as a non-destructive technique, could resolve well-defined stacks (sharp interfaces) deposited by magnetron sputtering. Multilayer systems down to 5 nm individual thickness were properly resolved by RBS. The powerful theoretical and simulation tools available for this technique allowed correction for mixing (i.e. straggling) effects. Improvement in RBS resolution down to the sub-nm range can be achieved by using magnetic spectrometer systems.

Artifacts related to the sputtering process were found when depth profiling by GDOES and SIMS, giving rise to interface-widening effects, which strongly depended on the nature of material and the depth of the analyzed layer.

Rough interfaces were detected by GDOES and SIMS better than by RBS due to the longer tails in the profiles. Both GDOES and SIMS could resolve ultra-thin layers

(down to 2.5 nm) of Cr in buried deep in structures (>1 μm). In general, SIMS showed interface degradation with depth much lower than GDOES, although the nm layers at the outermost surface could not be properly resolved. The use of Cs ions as bombarding species could increase the depth resolution further because the mass of the primary ion is greater [62].

The main effects contributing to the decrease in the depth resolution by GDOES were found to be ion-induced surface roughening and the resulting crater geometry giving rise to layer mixing when the individual layer thickness decreased. A particular characteristic of GDOES was that the different interface widening depended on the order on the layer materials (X/Y ≠ Y/X).

We expect that application of deconvolution algorithms would improve GDOES depth profiles.

As a final comment, it is clear from this review that, in multilayer nm depth profiling, no surface-analysis technique stands out. The choice of technique would depend on different factors (e.g., the system to be studied, the accuracy to be achieved, and the experimental time required). GDOES appears to be the most suitable technique for a rapid analysis, enabling feedback in the development process, though, for more accurate characterization, complementary analysis by RBS and/or SIMS would be necessary.

Acknowledgments

The authors wish to thank P. Chapon (Jobin–Yvon) and N. Bordel (Universidad de Oviedo) for their valuable comments during the preparation of the manuscript. This work was financially supported by the Spanish Ministry of Science and Innovation (project FUNCOAT CSD2008-00023).

References

[1] J. Musil, Surf. Coat. Technol. 125 (2000) 322.
[2] S. Veprek, M.G.J. Veprek-Heijman, P. Karvankova, J. Prochazka, Thin Solid Films 476 (2005) 1.
[3] J. Milano, A.M. Llois, L.B. Steren, A. Butera, J. Barnard, J. Appl. Phys. 96 (2004) 7392.
[4] P.S. Normile, J.A. De Toro, T. Muñoz, J.A. González, J.P. Andrés, P. Muñiz, R. Escobar Galindo, J.M. Riveiro, Phys. Rev. B 76 (2007) 104430.
[5] K. Chiba, T. Takahashi, Appl. Surf. Sci. 246 (2005) 48.
[6] F. Flory, L. Escoubas, Prog. Quantum Electron. 28 (2004) 89.
[7] H.W. Werner, R.P.H. Garten, Rep. Prog. Phys. 47 (1984) 221.
[8] R. Checchetto, C. Tosello, A. Miotello, G. Principi, J. Phys.: Condens. Matter 13 (2001) 811.
[9] C.J. Tavares, L. Rebouta, E. Alves, N.P. Barradas, J. Pacaud, J.P. Rivière, Nucl. Instrum. Methods Phys. Res., Sect. B 188 (2002) 90.
[10] P. Prieto, C. Morant, A. Climent-Font, A. Muñoz, E. Elizalde, J.M. Sanz, J. Vacuum Sci. Technol., A 24 (2006) 250.
[11] R. Escobar Galindo, E. Forniés, R. Gago, J.M. Albella, J. Anal. At. Spectrom. 22 (2007) 1512.
[12] E.H. Cirlin, Thin Solid Films 220 (1992) 197.
[13] C. Rincón, G. Zambrano, A. Carvajal, P. Prieto, H. Galindo, E. Martínez, A. Lousa, J. Esteve, Surf. Coat. Technol. 148 (2001) 277.
[14] C. Hongo, M. Tomita, M. Takenaka, A. Murakoshi, Appl. Surf. Sci. 203–204 (2003) 264.
[15] M.R. Winchester, R. Payling, Spectrochim. Acta, Part B 59 (2004) 607.
[16] N.H. Bings, A. Bogaerts, J.A.C. Broekaert, Anal. Chem. 80 (2008) 4317.
[17] W.B. Teo, K. Hirokawa, Surf. Interface Anal. 14 (1989) 143.
[18] Z. Weiss, Surf. Interface Anal. 15 (1990) 775.
[19] Z. Weiss, Spectrochim. Acta, Part B 47 (1992) 859.
[20] S. Oswald, S. Baunack, Thin Solid Films 425 (2003) 9.
[21] F. Präßler, V. Hoffmann, J. Schumann, K. Wetzig, J. Anal. At. Spectrom. 10 (1995) 677.
[22] V. Hodoroaba, W.E.S. Unger, H. Jenett, V. Hoffmann, B. Hagenhoff, S. Kayser, K. Wetzig, Appl. Surf. Sci. 179 (2001) 30.
[23] R. Payling, J. Michler, M. Aeberhard, Surf. Interface Anal. 33 (2002) 472.
[24] J. Michler, M. Aeberhard, D. Velten, S. Winter, R. Payling, J. Breme, Thin Solid Films 447–448 (2004) 278.
[25] R. Escobar Galindo, E. Forniés, J.M. Albella, J. Anal. At. Spectrom. 20 (2005) 1108.
[26] R. Escobar Galindo, E. Forniés, J.M. Albella, J. Anal. At. Spectrom. 20 (2005) 1116.
[27] V. Hoffmann, R. Dorka, L. Wilken, V.D. Hodoroaba, K. Wetzig, Surf. Interface Anal. 35 (2003) 575.
[28] A. Quentmeier, in: R. Payling, D.G. Jones, A. Bengston (Editors), Glow Discharge Optical Emission Spectroscopy, John Wiley & Sons, Chichester, West Sussex, UK, 1997 Sect. 7.1, 7.2.
[29] J. Angeli, A. Bengston, A. Bogaerts, V. Hoffmann, V. Hodoroaba, E. Steers, J. Anal. At. Spectrom. 18 (2003) 670.
[30] V.D. Hodoroaba, V. Hoffmann, E.B.M. Steers, M. Griepentrog, A. Dück, U. Beck, J. Anal. At. Spectrom. 21 (2006) 74.
[31] S. Baunack, V. Hoffmann, W. Zahn, Microchim. Acta 156 (2007) 69.
[32] A. Thobor, C. Rousselot, S. Mikhailov, Surf. Coat. Technol. 174–175 (2003) 351.
[33] A. Quentmeier, in: R. Payling, D.G. Jones, A. Bengston (Editors), Glow Discharge Optical Emission Spectroscopy, John Wiley & Sons, Chichester, West Sussex, UK, 1997 Sect. 7.3.
[34] Z. Weiss, in: R. Payling, D.G. Jones, A. Bengston (Editors), Glow Discharge Optical Emission Spectroscopy, John Wiley & Sons, Chichester, West Sussex, UK, 1997 Section 7.5.
[35] U. Beck, G. Reiners, Th. Wirth, V. Hoffmann, F. Präßler, Thin Solid Films 290–291 (1996) 57.
[36] K. Shimizu, G.M. Brown, H. Habazaki, K. Kobayashi, P. Skeldon, G.E. Thompson, G.C. Wood, Surf. Interface Anal. 27 (1999) 24.
[37] K. Shimizu, G.M. Brown, H. Habazaki, K. Kobayashi, P. Skeldon, G.E. Thompson, G.C. Wood, Electrochim. Acta 44 (1999) 2297.
[38] K. Shimizu, H. Habazaki, P. Skeldon, G.E. Thompson, Spectrochim. Acta, Part B 58 (2003) 1573.
[39] K. Shimizu, H. Habazaki, P. Skeldon, G.E. Thompson, Surf. Interface Anal. 35 (2003) 564.
[40] K. Shimizu, H. Habazaki, P. Skeldon, G.E. Thompson, R.K. Marcus, Surf. Interface Anal. 31 (2001) 869.
[41] S. Oswald, V. Hoffmann, G. Ehrlich, Spectrochim. Acta, Part B 49 (1994) 1123.
[42] S. Hofmann, in: D. Briggs, M.P. Seah (Editors), Practical Surface Analysis by Auger and X-ray Photoelectron Spectroscopy, John Wiley & Sons, Chichester, West Sussex, UK, 1983 Chap. 4.
[43] S. Hofmann, Surf. Interface Anal. 27 (1999) 825.
[44] J. Pisonero, B. Fernández, R. Pereiro, N. Bordel, A. Sanz-Medel, Trends Anal. Chem. 25 (2006) 11.
[45] M.A. Auger, R. Gago, M. Fernández, O. Sánchez, J.M. Albella, Surf. Coat. Technol. 157 (2002) 26.

[46] A. Climent-Font, F. Pászti, G. García, M.T. Fernández-Jiménez, F. Agulló, Nucl. Instrum. Methods Phys. Res., B 219–220 (2004) 400.
[47] D.F. Herring, R. Chiba, B.R. Gasten, H.T. Richards, Phys. Rev. 112 (1958) 1210.
[48] M. Mayer, SIMNRA User's Guide, IPP Report 9/113, Max-Planck-Institut für Plasmaphysik, Garching, Germany, 1997.
[49] http://www.jobinyvon.com
[50] V. Hoffmann, M. Kasik, P.K. Robinson, C. Venzago, Anal. Bioanal. Chem. 381 (2005) 173.
[51] J. Romero, A. Lousa, E. Martínez, J. Esteve, Surf. Coat. Technol. 163–164 (2003) 392.
[52] R. Escobar Galindo, J.M. Albella, Spectrochim. Acta, Part B 63 (2008) 422.
[53] P.H. Van Cittert, Z. Phys. 69 (1931) 298.
[54] R. Gold, ANL-6984, Argonne National Laboratories, Argonne, IL, USA, 1964.
[55] P. Bandžuch, M. Morháč, J. Krištiak, Nucl. Instrum. Methods Phys. Res., A 384 (1997) 506.
[56] B.W. Schueler, D.F. Reich, J. Vac. Sci. Technol., B 18 (2000) 496.
[57] W.M. Arnoldbik, W. Wolfswinkel, D.K. Inia, V.C.G. Verleun, S. Lobner, J.A. Reinders, F. Labohm, D.O. Boerma, Nucl. Instrum. Methods Phys. Res., B 118 (1996) 566.
[58] K. Kimura, S. Joumori, Y. Oota, K. Nakajima, M. Suzuki, Nucl. Instrum. Methods Phys. Res., B 219–220 (2004) 351.
[59] R. Andrzejewski, J. Lucas, A. Guirao, N. Gordillo, D.O. Boerma, Nucl. Instrum. Methods Phys. Res., B 249 (2006) 939.
[60] R. Nagel, C. Alof, A.G. Balogh, W.M. Arnoldbik, D.O. Boerma, Nucl. Instrum. Methods Phys. Res., B 183 (2001) 140.
[61] S. Hosoi, K. Nakajima, M. Suzuki, K. Kimura, Y. Shimizu, S. Fukatsu, K.M. Itoh, M. Uematsu, H. Kageshim, K. Shiraishi, Nucl. Instrum. Methods Phys. Res., B 249 (2006) 390.
[62] M. Tomita, M. Suzuki, T. Tachibe, S. Kozuka, A. Murakoshi, Appl. Surf. Sci. 203–204 (2003) 377.